

A&A manuscript no.
(will be inserted by hand later)
Your thesaurus codes are:
08 (08.09.2 Sirius A; 08.09.2 Sirius B; 08.23.1; 09.01.1; 13.21.3; 13.21.5)

**ASTRONOMY
AND
ASTROPHYSICS**

Ultraviolet observations of Sirius A and Sirius B with HST-GHRS *

An interstellar cloud with a possible low deuterium abundance

G. Hébrard^{1,2}, C. Mallouris³, R. Ferlet¹, D. Koester⁴, M. Lemoine⁵, A. Vidal-Madjar¹, and D. York³

¹ Institut d'Astrophysique de Paris, CNRS, 98 bis Boulevard Arago, F-75014 Paris, France

² Department of Physics and Astronomy, Johns Hopkins University, 3400 North Charles Street, Baltimore, MD 21218, USA

³ University of Chicago, Department of Astronomy and Astrophysics, 5640 South Ellis Avenue, Chicago, IL 60637, USA

⁴ Institut für Theoretische Physik und Astrophysik der Christian-Albrechts-Universität, D-24098 Kiel, Germany

⁵ DARC, UPR-176 CNRS, Observatoire de Paris-Meudon, F-92195 Meudon Cédex, France

Received ? / Accepted ?

Abstract. We present new observations of the binary Sirius A / Sirius B performed with HST-GHRS. Two interstellar clouds are detected on this sightline, one of them being identified as the Local Interstellar Cloud (LIC), in agreement with previous HST-GHRS observations of Sirius A (Lallemand et al. 1994). The interstellar structure of this sightline, which we assume is the same toward both stars (separated by less than 4 arcsec at the time of observation), is constrained by high spectral resolution data of the species O I, N I, Si II, C II, Fe II and Mg II.

Lyman α interstellar lines are also observed toward the two stars. But whereas the deuterium Lyman α line is well detected in the LIC with an abundance in agreement with that obtained by Linsky et al. (1993 & 1995), no significant D I line is detected in the other cloud.

However, the Lyman α lines toward Sirius A and Sirius B are not trivial. An excess of absorption is seen in the blue wing of the Sirius A Lyman α line and interpreted as the wind from Sirius A. In its white dwarf companion, an excess in absorption is seen in the red wing and interpreted as the core of the Sirius B photospheric Lyman α line. A composite Lyman α profile can nonetheless be constructed, and allows one to measure the deuterium abundance in the second cloud $0 < (D/H)_{ISM} < 1.6 \times 10^{-5}$, which is marginally in agreement with the Linsky et al. (1993 & 1995) value. This sightline appears consequently as a good candidate for a low $(D/H)_{ISM}$.

Key words: Stars: individual: Sirius A – Stars: individual: Sirius B – Stars: white dwarfs – ISM: abundances – Ultraviolet: ISM – Ultraviolet: stars.

1. Introduction

It is generally believed that deuterium is only produced in primordial Big Bang nucleosynthesis (BBN), and destroyed in stellar interiors (Epstein, Lattimer & Schramm 1976). Hence, any abundance of deuterium measured at any metallicity should provide a lower limit to the primordial deuterium abundance (Reeves et al. 1973). Deuterium is thus a key element in cosmology and in galactic chemical evolution (e.g., Vangioni-Flam & Cassé 1995; Prantzos 1996; Scully et al. 1997). The primordial abundance of deuterium is indeed one of the best probes of the baryonic density parameter of the Universe Ω_B . The decrease of its abundance all along galactic evolution, amongst other things, is a function of the star formation rate. Standard models predicting a decrease by a factor 2 to 3 in 15 Gyrs (e.g., Galli et al. 1995; Prantzos 1995; Tosi et al. 1998). However there are some non-standard models which propose nonprimordial deuterium production (see e.g. Lemoine et al. (1999) for a review). The most recent paper on nonprimordial deuterium production is by Mullan & Linsky (1999).

Proto-solar and interstellar deuterium abundances thus bear the imprint of BBN as well as the subsequent chemical evolution. Up to a few years ago, they were the only available measurements of D/H used to constrain BBN in a direct way. The situation has changed recently, as measurements of D/H likely to be close to $(D/H)_{prim}$ have become possible (e.g., Burles & Tytler 1998a & 1998b; Webb et al. 1997; see also Burles & Tytler 1998c for a review). Taken altogether, the abundances of deuterium seem to decrease with time, as expected, although the dispersion

Send offprint requests to: Guillaume Hébrard

* Based on observations with the NASA/ESA *Hubble Space Telescope*, obtained at the Space Telescope Science Institute, which is operated by the Association of Universities for Research in Astronomy, Inc. under NASA contract No. NAS5-26555.

Correspondence to: hebrard@iap.fr

remains rather large. These various measurements and their trends are reviewed in detail in Lemoine et al. (1999), and we refer the reader to this review for more details.

The first measurements of the interstellar deuterium abundance $(D/H)_{ISM}$, representative of the present epoch, were reported by Rogerson & York (1973) through Lyman absorption on the line of sight of β Cen, using *Copernicus*. Their value of $(D/H)_{ISM} \simeq 1.4 \pm 0.2 \times 10^{-5}$ has not changed ever since and twenty years later, Linsky et al. (1993 & 1995) measured $(D/H)_{ISM} = 1.60 \pm 0.09^{+0.05}_{-0.10} \times 10^{-5}$ in the direction of Capella using HST-GHRS. But it turns out that determinations of the $(D/H)_{ISM}$ ratio do not generally agree on a single value, even in the very local medium (Vidal-Madjar et al. 1978 & 1986, Murthy et al. 1987 & 1990). While many measurements are in agreement with the value of Linsky et al. (1993 & 1995), many sightlines exhibit different values. For instance, $(D/H)_{ISM} < 10^{-5}$ toward λ Sco (York 1983), $(D/H)_{ISM} \simeq 7. \times 10^{-6}$ toward δ Ori and ϵ Ori (Laurent et al. 1979), $(D/H)_{ISM} \simeq 5. \times 10^{-6}$ toward θ Car (Allen et al. 1992). Finally, thanks to new HST-GHRS observations of G191-B2B, Vidal-Madjar et al. (1998) detected variations of $(D/H)_{ISM}$ by at least $\sim 30\%$ within the local interstellar medium on the sightline of G191-B2B, and Jenkins et al. (1999) up to $\sim 50\%$ toward δ Ori, using IMAPS. We can also report the measurement of the 92cm hyperfine transition of D I by Chengalur et al. (1997), showing $(D/H)_{ISM} \simeq 3.9 \pm 1.0 \times 10^{-5}$. Although several scenarios have been proposed to explain these putative variations (e.g., Vidal-Madjar et al. 1978; Jura 1982), the above measurements are still unaccounted for (Lemoine et al. 1999).

We introduced in Cycle 1 of HST a new type of target, white dwarfs in the high temperature range, for which the depth of the Lyman α photospheric absorption line is reduced, and whose stellar continuum remains smooth. These targets also allow the study of lines of other species, such as N I and O I, which are shown to be reliable tracers of H I in the ISM (Ferlet 1981; York et al. 1983). These targets may also be chosen close to the Sun so that the H I column density is not too high and the velocity structure of the line of sight not too complex. We have already observed the white dwarf G191-B2B in HST Cycle 1 (Lemoine et al. 1996) and Cycle 5 (Vidal-Madjar et al. 1998). Continuing that program, we present here new ultraviolet observations of Sirius A and its white dwarf companion Sirius B performed with HST-GHRS. Previous HST-GHRS observations of Sirius A reveal the velocity structure including two components on this sightline (Lallemand et al. 1994), and also the possible detection of a diffuse interstellar cloud boundary (Bertin et al. 1995a) and the detection of a stellar wind from Sirius A (Bertin et al. 1995b).

From a subset of these new observations, the identifications of the Sirius A emission lines have been made beforehand (van Noort et al. 1998). Here, following the presentation of these spectroscopic observations and the

data reduction in Section 2, we study the structure of the line of sight in Section 3, the Lyman α absorption features including D/H study in Section 4, and the ionization and metal abundances in Section 5. We finally discuss our results in Section 6.

2. Observations and data reduction

2.1. Observations

Our observations of the stars Sirius A and Sirius B were performed with GHRS (the *Goddard High Resolution Spectrograph*) onboard the *Hubble Space Telescope* in November 1996, in the frame of Cycle 6 Guest Observer proposals ID 6800 and ID 6828. A first attempt was made in September 1996 but failed because the stars were not correctly located within the GHRS entrance slit. The observations were finally repeated with a different pointing strategy which was fully successful and allowed for extremely good observations of both stars. The spectra were acquired at high and medium spectral resolution (Echelle-A and G140M gratings). Most of them have a very good quality and show clearly interstellar lines. The wavelengths ranges of the spectra are listed in Table 1.

The G140M grating provides a resolving power $R = \lambda/\Delta\lambda \simeq 20,000$, *i.e.* a spectral resolution of $\sim 15 \text{ km s}^{-1}$. With the Echelle-A grating we have obtained a resolving power $R \simeq 85,000$, *i.e.* a spectral resolution of $\sim 3.5 \text{ km s}^{-1}$. We used only the Small Science Aperture (SSA), corresponding to $0.25''$ on the sky and illuminating one diode to achieve the best possible resolving power. For further details on the instrumentation, see Duncan (1992).

2.2. Data reduction

Our data were reduced with the Image Reduction and Analysis Facility (IRAF) software, using the STSDAS package.

During the observations, we used the FP-SPLIT mode which splits the total exposure time into successive cycles of four sub-exposures, each corresponding to a slightly different projection of the spectrum on the photocathode. We used the “quarter stepping” mode, which provides a sample of 4 pixels per resolution element. This allows simultaneously to oversample the spectrum, since, for instance, the SSA does not fulfill the Nyquist sampling criterion, and to correct for the granularity of the photocathode. The effect of the photocathode on each diode being the same for the four sub-exposures, it is possible to evaluate this granularity from the comparison of the four sub-exposures where a constant granularity effect mixes with a non-constant photon statistical noise.

We use several methods to average the four series of sub-exposures to obtain the final spectra. The main point

Table 1. List of our GHRS spectra.

Target	Spectral range	Elements	GHRS Grating	Exposition time	Date of observation	Proposal	#
Sirius A	1188 Å - 1218 Å	N I, Si II, Si III, H I, D I	G140M	1632.0 s	1996 Nov. 20	ID 6800	1
Sirius A	1278 Å - 1307 Å	O I, Si II	G140M	217.6 s	1996 Nov. 20	ID 6800	2
Sirius A	1308 Å - 1337 Å	C II	G140M	217.6 s	1996 Nov. 20	ID 6800	3
Sirius A	1196 Å - 1203 Å	N I	Echelle-A	1305.6 s	1996 Nov. 20	ID 6800	4
Sirius A	1201 Å - 1208 Å	Si III	Echelle-A	870.4 s	1996 Nov. 20	ID 6800	5
Sirius A	1298 Å - 1306 Å	O I, Si II	Echelle-A	130.2 s	1996 Nov. 20	ID 6800	6
Sirius A	1331 Å - 1339 Å	C II	Echelle-A	217.6 s	1996 Nov. 20	ID 6800	7
Sirius B	1188 Å - 1218 Å	N I, Si II, Si III, H I, D I	G140M	1532.8 s	1996 Nov. 18	ID 6828	8
Sirius B	1278 Å - 1307 Å	O I, Si II	G140M	217.6 s	1996 Nov. 18	ID 6828	9
Sirius B	1308 Å - 1337 Å	C II	G140M	217.6 s	1996 Nov. 18	ID 6828	10
Sirius B	1196 Å - 1203 Å	N I	Echelle-A	3481.6 s	1996 Nov. 21	ID 6800	11
Sirius B	1201 Å - 1208 Å	Si III	Echelle-A	1740.8 s	1996 Nov. 18	ID 6828	12
Sirius B	1212 Å - 1219 Å	H I, D I	Echelle-A	2067.2 s	1996 Nov. 18	ID 6828	13
Sirius B	1212 Å - 1219 Å	H I, D I	Echelle-A	3481.6 s	1996 Nov. 20	ID 6800	14
Sirius B	1298 Å - 1306 Å	O I, Si II	Echelle-A	217.6 s	1996 Nov. 18	ID 6828	15
Sirius B	1331 Å - 1339 Å	C II	Echelle-A	217.6 s	1996 Nov. 18	ID 6828	16

was to focus the alignment between the different sub-exposures, in order to avoid any artificial broadening of the lines, or even erasing the weaker ones. Where the signal-to-noise ratio (S/N) was high enough, we used the standard method to average the sub-exposures and correct for the granularity, which is available in the IDL GHRS package, under the *corre-hrs* procedure. This procedure, which executes an automatic auto-correlation between the sub-exposures, is efficient when the sub-exposures are bright enough. We found that this simple treatment allowed us to reach good alignment for ten of our spectra (spectra # 1, 2, 3, 4, 6, 7, 8, 9, 10 and 15 in Table 1). In the remaining cases the S/N was too low, and the *corre-hrs* procedure was not able to identify and then correlate features on the sub-exposures. For these six low S/N spectra (spectra # 5, 11, 12, 13, 14 and 16 in Table 1), we chose to estimate the shifts between the different sub-exposures one by one, after smoothing them in order to increase the S/N , and then to average the sub-exposures with the right shifts (and with no additional smoothing). The shifts found thus were very close to the nominal ones in the FP-SPLIT mode. However these six low S/N spectra are not corrected for the photocathode granularity. Instead we have searched for such possible defects by adding the sub-exposures corresponding a priori to the same spectral instrument shift, improving then the S/N , and building in such a way four different shifted spectra where the photocathode defects appear at fixed positions. We found no defects near the observed spectral lines. This can be seen, for example, in the Fig. 1 and Fig. 2 on which are shown the Sirius A and Sirius B Echelle-A data corresponding to both C II 1334 Å and O I 1302 Å areas.

In our high and medium spectral resolution data, we have detected 10 interstellar lines toward Sirius A and/or Sirius B: N I 1200 Å triplet, O I 1302 Å, C II 1334 Å, Si II

1190 Å, 1193 Å and 1304 Å, D I 1215 Å and H I Lyman α (see Table 2).

To properly deduce interstellar abundances from interstellar absorption lines, it is extremely important to precisely evaluate the zero flux level. The zero flux level may be slightly erroneous due to the scattered light, which is greater in the case of an échelle grating like Echelle-A than in the case of a classical grating like G140M, because of the diffuse light produced from the adjacent spectral orders. Thus, under the two assumptions that the zero flux is well known for G140M spectra, and that the width of the line spread function with Echelle-A is negligible in comparison with the one obtained with G140M, we used the G140M spectra to adjust the zero level of the corresponding Echelle-A spectra (for example, we adjust spectrum # 15 with # 9, spectrum # 16 with # 10...). Accordingly, after degrading the Echelle-A spectrum to the one of G140M *i.e.* projection of Echelle-A spectrum on pixels with size equal to those of G140M spectrum, and then convolution with the G140M line spread function), we achieve the flux shift between the degraded Echelle-A spectrum and the corresponding G140M one. We corrected thus the zero flux levels of the non-degraded Echelle-A spectra with these shifts, in the cases of unsaturated lines. The most obvious cases are the broad and saturated Lyman α lines for which the central saturated cores should be at zero flux level. We shift these spectra in order to adjust the Lyman α central cores at zero flux level (the level of that core has been found to be negative after the standard pipeline correction). This obvious case allows us to test and confirm that the zero flux level is well known in G140M spectra. It permits to ensure that the precision on the zero flux level for the G140M spectra, and thus for the corrected Echelle-A ones, is better than 3% of the stellar continuum.

Seven of the Echelle-A exposures (# 4, 5, 12, 13, 14, 15 and 16) were immediately preceded by a platinum lamp

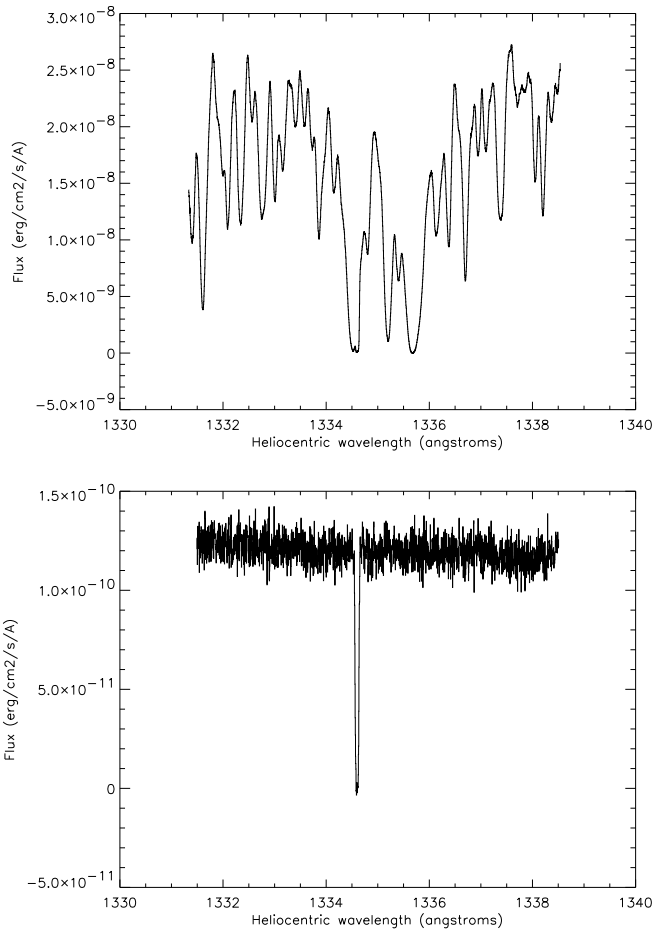


Fig. 1. Examples of spectra obtained with HST-GHRS Echelle-A: C II area toward Sirius A (top, spectrum # 7) and toward Sirius B (bottom, spectrum # 16). In the Sirius A spectrum we see a lot of stellar lines, and an interstellar absorption on the red wing of the C II 1334.5 Å stellar line. In the Sirius B spectrum we see only the interstellar C II 1334.5 Å line on a very flat stellar continuum.

calibration exposure and thus allowed us to calculate the residual wavelength shift left by the standard *calib_hrs* calibration procedure. Together with the oversampling mode, this correction allowed us to reach an absolute calibration accuracy of $\pm 1.5 \text{ km s}^{-1}$ in radial velocity (the radial velocities will thereafter be given in heliocentric frame).

We chose not to rebin our spectra *i.e.* they present four pixels per resolution element approximately, which is the standard sampling mode. For our fits (§ 3 and § 4) we then used a gaussian PSF, with a FWHM slightly greater than four pixels.

In order to study the interstellar contributions, the regions near the interstellar spectral lines were normalized by the stellar continuum to unity. This could be done without difficulty, except in the case of the Lyman α line toward Sirius B, with polynomial whose degree and parameters were chosen using the procedure described in

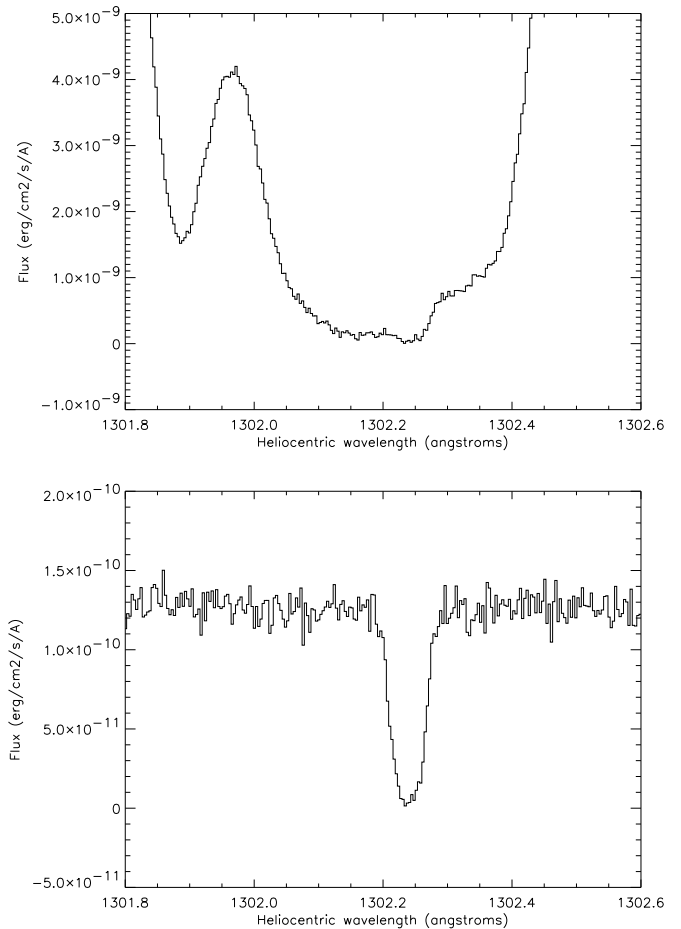


Fig. 2. Examples of spectra obtained with HST-GHRS Echelle-A (magnification): O I area toward Sirius A (top, spectrum # 6) and toward Sirius B (bottom, spectrum # 15). On the Sirius A spectrum, the interstellar absorption line (the small feature at 1302.25 Å) is at the bottom of a stellar line. For this small feature, the continuum is low and less simple than in the case of Sirius B spectrum, on which we see only the interstellar line, on a very flat stellar continuum.

Lemoine et al. (1995). The photospheric Lyman α continua of Sirius B was non-trivial and its normalization will be described in § 4.

The Lyman α high resolution spectra of Sirius A obtained using Echelle-A was unusable, probably because of the very high diffusion of adjacent order in the spectrograph by this bright star. The Lyman α high resolution spectra of Sirius B obtained using Echelle-A presented a very low S/N (~ 5). We did not use them in our fits of the Lyman α lines (§ 4), which are made only on the medium spectral resolution data obtained using G140M. We just use them in order to check that the geocoronal Lyman α emission during our observations was at the bottom of the saturated Lyman α absorptions. Indeed, this emission is detected in the Sirius B Lyman α Echelle-A spectra, but

not in the G140M spectra. The geocoronal emission thus did not deteriorate the wings of the Lyman α absorption lines.

3. Structure of the line of sight

As it can be seen in § 4, the Lyman α lines are not obvious. We thus used only the interstellar metal lines (*i.e.* all but Lyman α) to study the structure of the line of sight toward the binary Sirius A / Sirius B. We assume in all our study that the interstellar absorbers are the same toward Sirius A and Sirius B, the two stars being separated by less than 4 arcsec on the sky at the time of our observations, which corresponds to ~ 10 AU at the Sirius distance of 2.6 pc.

For a given transition of a given element, each component in the sightline produces an absorption line modeled by a Voigt profile, which is defined, in addition to atomic parameters, by four cloud parameters: the radial velocity v (in km s^{-1}) of the cloud, the column density N_e (in cm^{-2}) of element e , the temperature T (in K) of the gas, and its turbulent velocity σ (in km s^{-1}).

In order to determine the number of clouds, their velocity, temperature, turbulence and columns density for each element, we used a new fitting program developed by M. Lemoine, which permits to fit Voigt profiles to several lines in different spectral ranges simultaneously. This new program works in the same spirit as the code presented in Lemoine et al. (1995), which obtains the best fit by χ^2 simulated annealing optimization. This allows us to find the best solution compatible with different spectral ranges based on the basic assumption that all the considered lines give the same values for v , T and σ for a given component, and all the lines for a given element e and a given component give the same value for N_e . The spread of the lines combines both parameters T and σ , which can only be separately determined if several elements with different masses are simultaneously fitted. This procedure was used to solve the structure of the line of sight toward the white dwarf G191-B2B (Vidal-Madjar et al. 1998).

The previous study of the line of sight toward Sirius A (Lallemand et al. 1994) clearly showed two distinct interstellar clouds with a projected velocity shift equal to $5.7 \pm 0.2 \text{ km s}^{-1}$. The red component was identified as the Local Interstellar Cloud (LIC), detected in many directions with projected velocities corresponding to the coherent motion of a cloud in which the solar system is embedded (Lallemand & Bertin 1992). To improve the precision of our study, we decided to fit the 10 lines of our new observation together with the Fe II 2344 Å, Fe II 2600 Å, Mg II 2796 Å and Mg II 2803 Å lines from Lallemand et al. (1994), which present very high S/N (see Table 2).

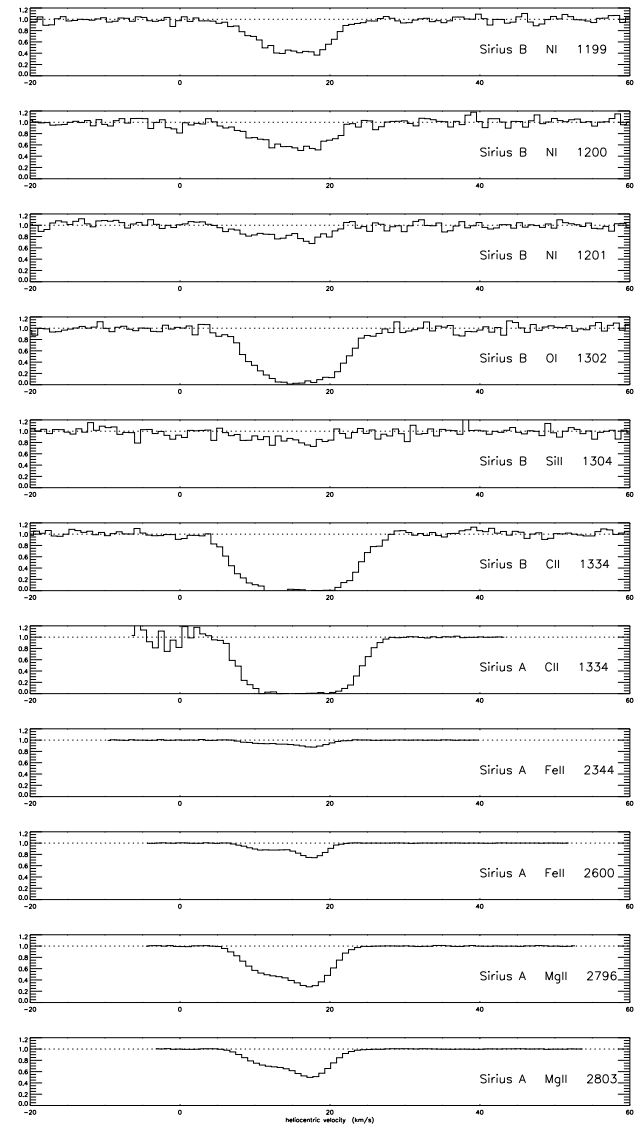


Fig. 3. High resolution interstellar lines toward Sirius A and Sirius B after velocity shifts correction (solid lines), and normalized stellar continuum (dotted lines).

3.1. Velocity shifts correction

Our fitting program is suitable for a simultaneous study of several lines with the restriction that their wavelengths are precisely determined. If there exist significant velocity shifts between different lines caused for instance, by instrumental effects, the program then becomes unable to find the right solution coherent with all the fitted lines. Therefore, on a first iteration, we have corrected for any possible instrumental velocity shifts.

In order to estimate the values of these instrumental shifts, we decided to begin our study by fitting one by one all the lines, assuming that there were two components, the blue one (BC) and the red one (LIC), with the following constraints:

Table 2. Interstellar spectral lines detected on HST-GHRS spectra toward Sirius A and Sirius B. S/N is the signal to noise ratio per pixel at the continuum of the interstellar lines. The atomic data are from Morton (1991).

Element	Wavelength (Å) (vacuum)	Oscillator strength	Spontaneous transition probability (s^{-1})	Target	Spectral resolution	S/N	Reference
N I	1199.5496	1.328×10^{-1}	4.104×10^8	Sirius A	85,000	5	This work
				Sirius B	20,000	40	This work
				Sirius B	85,000	20	This work
N I	1200.2233	8.849×10^{-2}	4.097×10^8	Sirius A	85,000	5	This work
				Sirius B	20,000	45	This work
				Sirius B	85,000	20	This work
N I	1200.7098	4.423×10^{-2}	4.093×10^8	Sirius A	85,000	5	This work
				Sirius B	20,000	35	This work
				Sirius B	85,000	15	This work
O I	1302.1685	4.887×10^{-2}	3.204×10^8	Sirius A	85,000	10	This work
				Sirius B	20,000	50	This work
				Sirius B	85,000	15	This work
C II	1334.5323	1.278×10^{-1}	2.393×10^8	Sirius A	85,000	50	This work
				Sirius B	20,000	40	This work
				Sirius B	85,000	20	This work
Si II	1190.4158	2.502×10^{-1}	5.888×10^8	Sirius B	20,000	50	This work
Si II	1193.2897	4.991×10^{-1}	2.338×10^9	Sirius B	20,000	45	This work
Si II	1304.3702	1.473×10^{-1}	5.776×10^8	Sirius A	85,000	10	This work
				Sirius B	20,000	45	This work
				Sirius B	85,000	15	This work
Fe II	2344.2141	1.097×10^{-1}	1.664×10^8	Sirius A	85,000	200	Lallement et al. (1994)
Fe II	2600.1729	2.239×10^{-1}	2.209×10^8	Sirius A	85,000	300	Lallement et al. (1994)
Mg II	2796.3521	6.123×10^{-1}	2.612×10^8	Sirius A	85,000	150	Lallement et al. (1994)
Mg II	2803.5310	3.054×10^{-1}	2.592×10^8	Sirius A	85,000	200	Lallement et al. (1994)
D I	1215.3394	4.165×10^{-1}	6.270×10^8	Sirius A	20,000	20	This work
				Sirius A	15,000	20	Lallement et al. (1994)
				Sirius B	20,000	10	This work
				Sirius B	85,000	5	This work
H I	1215.6701	4.164×10^{-1}	6.265×10^8	Sirius A	20,000	20	This work
				Sirius A	15,000	20	Lallement et al. (1994)
				Sirius B	20,000	10	This work
				Sirius B	85,000	5	This work

- $\Delta v_{\text{LIC-BC}} = 5.7 \text{ km s}^{-1}$,
- $1.5 \text{ km s}^{-1} \leq \sigma_{\text{BC}} \leq 3.5 \text{ km s}^{-1}$,
- $100 \text{ K} \leq T_{\text{BC}} \leq 10000 \text{ K}$,
- $0.1 \text{ km s}^{-1} \leq \sigma_{\text{LIC}} \leq 2.5 \text{ km s}^{-1}$,
- $T_{\text{LIC}} = 7000 \text{ K}$.

These values were the result of the Lallement et al. (1994) paper. The strong constraints were the projected velocity shift $\Delta v_{\text{LIC-BC}} = 5.7 \text{ km s}^{-1}$ exactly, which is the Lallement et al. (1994) result without the reported errors, and $T_{\text{LIC}} = 7000 \text{ K}$, which is the standard value assumed for the LIC [see for example Linsky et al. (1995)].

Each fit gives a pair of velocities, one for the BC and one for the LIC, separated by 5.7 km s^{-1} .

We did not find the same pairs of velocities for all the lines, and we interpreted these shifts as signs of instrumental errors in the absolute wavelength calibration. Indeed, the shift between the C II and O I lines, for which the spectra was preceded by a platinum lamp calibration exposure, was on the order of 1 km s^{-1} , rather than for the lines not

preceded by calibration exposures which presented greater shifts. We took as reference the average pair of velocities found with the spectra preceded by calibration exposures, and we shifted all our spectra by hand on this reference.

We thus fit together the lines of higher S/N and spectral resolution, and we obtained a first set of results for the values of v , T , σ and N_e for the two components. Fitting one by one the lower S/N or lower spectral resolution data with the constraints from these first results, we improved the velocity shift correction in the same spirit as above.

After this iterative process, there remained no instrumental velocity shift greater than $\pm 0.5 \text{ km s}^{-1}$ in our data, as it can be seen in Fig. 3 (high resolution data) and in Fig. 4 (medium resolution data). All the detected interstellar lines were thus well calibrated in wavelength, and ready to be fitted all together to constraint the sightline.

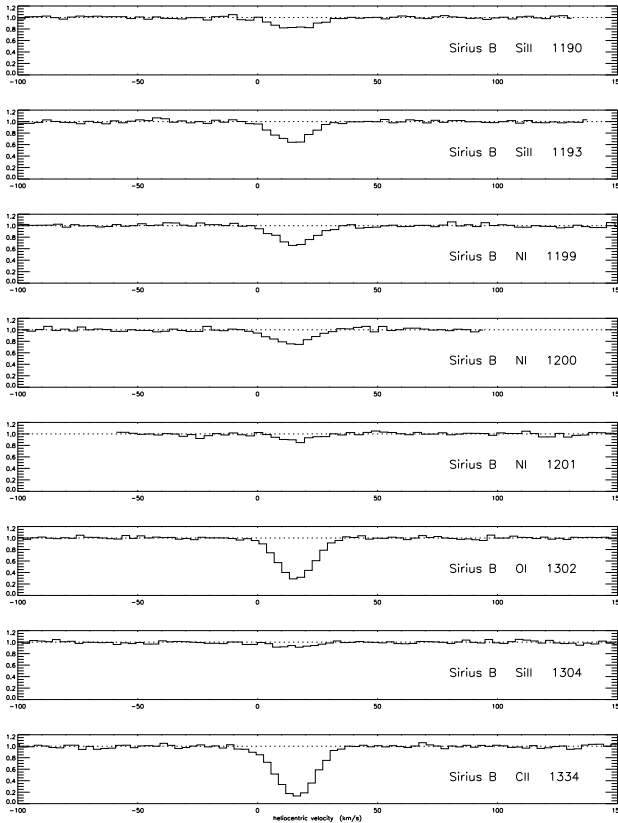


Fig. 4. Medium resolution interstellar lines toward Sirius B after velocity shifts correction (solid lines), and normalized stellar continuum (dotted lines).

3.2. Interstellar structure of the line of sight

We fitted together 19 high and medium spectral resolutions interstellar lines but this time without the hypotheses of § 3.1 on the radial velocity shift between the two clouds or on the widths of the lines. Assuming only that there are two components on the sightline, we let all the other parameters vary. We did not include in this fit the high spectral resolution interstellar lines N I, O I and Si II toward Sirius A due to their low S/N .

The values found from this global fit are reported in Table 3 and the fit plots in Fig. 5. The reduced χ^2 from this fit is 1.12 for 749 degrees of freedom. The error bars given in Table 3 are statistical $\pm 2\sigma$ errors according to the $\Delta\chi^2$ method. We checked them on the one hand by trial and error, and on the other hand by performing fits to all species but one, each species being excluded in turn, and comparing the obtained results.

Adopting the same method/procedure, but using a fitting program developed by D. Welty (Welty et al. 1991), we get very good agreement in the column densities, temperatures and velocity separation of BC and LIC.

The quality of the fit allows to affirm that there is no signature of an extra component on this line of sight.

Table 3. Results of the final fit of the 19 interstellar metal lines together (see plots in Fig. 5).

Component	BC	LIC
Temperature [K]	3000^{+2000}_{-1000}	8000^{+500}_{-1000}
Turb. velocity [km s^{-1}]	2.7 ± 0.3	0.5 ± 0.3
Radial velocity [km s^{-1}]	11.7 ± 1.5	17.6 ± 1.5
$\Delta v_{\text{LIC-BC}}$	$= 5.9 \pm 0.3$	
$N(\text{N I}) [\text{cm}^{-2}]$	$9.2^{+2.0}_{-1.0} \times 10^{12}$	$1.3^{+0.1}_{-0.2} \times 10^{13}$
$N(\text{O I}) [\text{cm}^{-2}]$	$5.0^{+1.5}_{-1.0} \times 10^{13}$	$3.4^{+1.5}_{-1.0} \times 10^{14}$
$N(\text{Si II}) [\text{cm}^{-2}]$	$2.7^{+1.0}_{-0.5} \times 10^{12}$	$3.0^{+1.0}_{-0.5} \times 10^{12}$
$N(\text{C II}) [\text{cm}^{-2}]$	$6.0^{+2.5}_{-1.5} \times 10^{13}$	$4.2^{+3.0}_{-2.0} \times 10^{14}$
$N(\text{Fe II}) [\text{cm}^{-2}]$	$5.5^{+0.4}_{-0.4} \times 10^{11}$	$8.7^{+0.3}_{-0.3} \times 10^{11}$
$N(\text{Mg II}) [\text{cm}^{-2}]$	$1.0^{+0.1}_{-0.1} \times 10^{12}$	$1.7^{+0.1}_{-0.1} \times 10^{12}$

Thus we assume in the following that there are only two interstellar clouds toward Sirius.

Our results are in agreement with those of Lallement et al. (1994), which provided for temperatures and turbulent velocities $T_{\text{LIC}} = 7600 \pm 3000$ K and $\sigma_{\text{LIC}} = 1.4^{+0.6}_{-1.4} \text{ km s}^{-1}$, and $T_{\text{BC}} = 1000^{+6000}_{-1000}$ K and $\sigma_{\text{BC}} = 2.9^{+0.1}_{-0.5} \text{ km s}^{-1}$. These two components were already also detected toward ϵ CMa which is located at 12° from Sirius (Gry et al. 1995), “component 2” in that study being the same as the one named here “BC”. The values by Gry et al. (1995) toward ϵ CMa are $T_{\text{LIC}} = 7200 \pm 2000$ K and $\sigma_{\text{LIC}} = 2.0 \pm 0.3 \text{ km s}^{-1}$, and $T_{\text{BC}} = 3600 \pm 1500$ K and $\sigma_{\text{BC}} = 1.85 \pm 0.3 \text{ km s}^{-1}$. The agreement is good for the temperatures, but less good for the turbulent velocities. Recent observations of the LIC given toward Capella $T_{\text{LIC}} = 7000 \pm 500 \pm 400$ K and $\sigma_{\text{LIC}} = 1.6 \pm 0.4 \pm 0.2 \text{ km s}^{-1}$ (Linsky et al. 1995), toward Procyon $T_{\text{LIC}} = 6900 \pm 80 \pm 300$ K and $\sigma_{\text{LIC}} = 1.21 \pm 0.27 \text{ km s}^{-1}$ (Linsky et al. 1995), and toward the white dwarf G191-B2B $T_{\text{LIC}} = 4000^{+2000}_{-1500}$ K and $\sigma_{\text{LIC}} = 2.0^{+0.5}_{-1.0} \text{ km s}^{-1}$ (Vidal-Madjar et al. 1998). Here, again the agreement with our values is good for temperature, but less good for turbulent velocity. That might suggest a different turbulent structure toward Sirius.

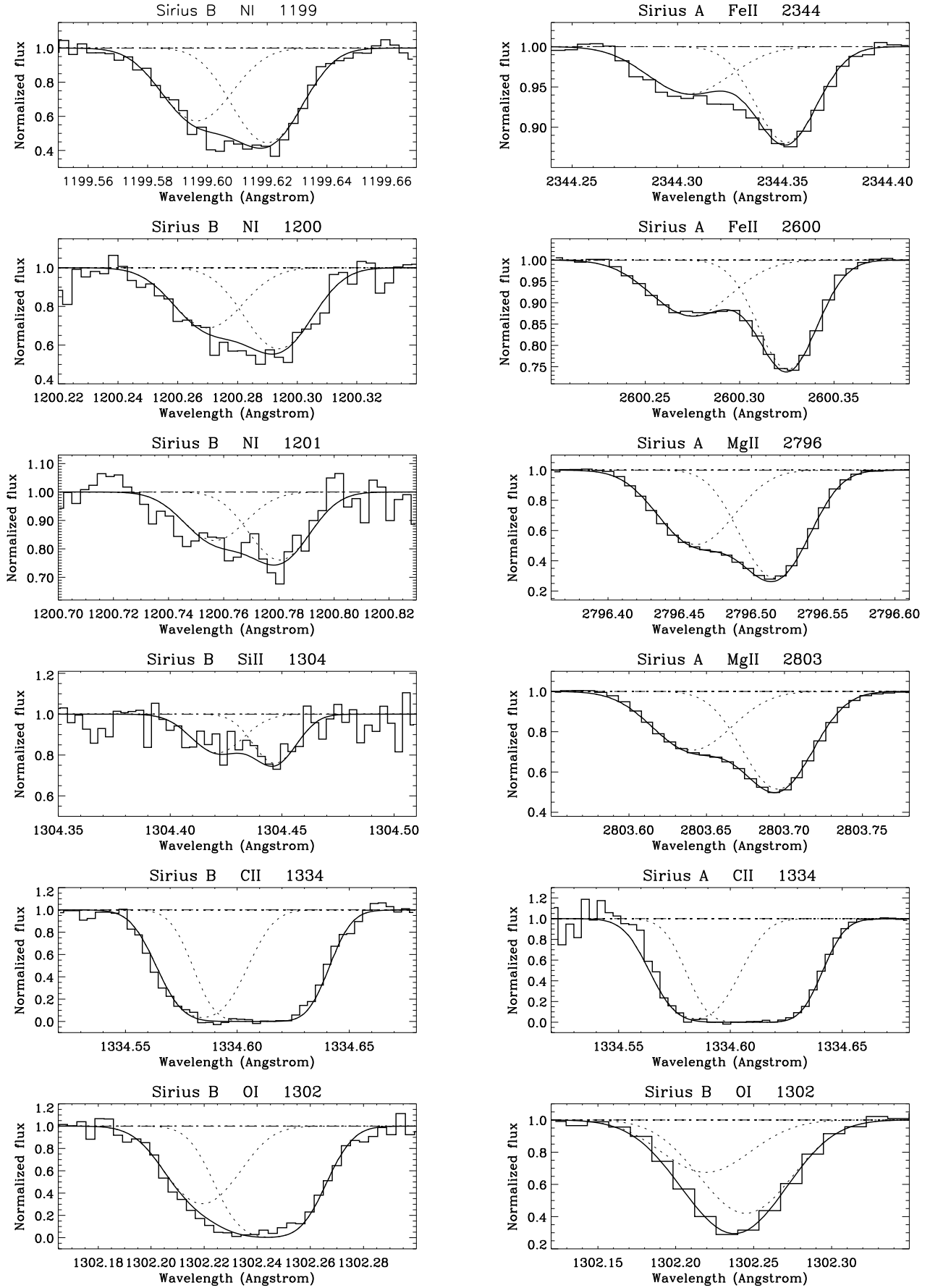


Fig. 5. The final fit for the metal lines toward Sirius B and Sirius A (see values found in Table 3). All the high spectral resolution lines are shown with their corresponding best fit (Sirius B, Sirius A, and reference).

4. Analysis of the Lyman α lines toward Sirius A and Sirius B

The problem of possible instrumental radial velocity shifts is the same for the Lyman α spectra here as with the metal lines above. Being in the same spectrum as the triplet N I, we corrected the Sirius B G140M Lyman α line by the shift found for that triplet. It was less obvious for the Sirius A G140M Lyman α line because the interstellar N I lines were not detected on this spectra due to the too low spectral resolution and S/N . But in spite of low S/N , the interstellar N I triplet was detected in the Sirius A Echelle-A spectra, on the red wings of the stellar N I lines. Thus it was possible to align the interstellar N I high resolution lines in the sightline of Sirius A with the equivalent high resolution lines in the sightline of Sirius B, for which instrumental velocity shifts were already corrected (see above). With N I triplet and Lyman α being on the same G140M spectrum, alignment of the Sirius A G140M N I triplet spectral zone with the Sirius A Echelle-A N I triplet spectral zone further permitted alignment of the Sirius A G140M Lyman α line.

However, a check on the deuterium absorption lines in the blue wings of both Lyman α lines indicates a velocity shift between the two spectra. It is probably due to the large wavelength coverage in G140M spectra between the N I and Lyman α lines and to the low S/N on the high resolution Sirius A N I spectrum, implying a coarse determination of interstellar component velocities. Here, using again the same strategy to correct velocity shifts, we fit one by one the two deuterium lines, assuming the results obtained above for the structure of the sightline. We found a shift 1.5 km s^{-1} between the two N I lines, a shift which was corrected by hand.

After all shift corrections, we estimate that the possible instrumental velocity shift between the Sirius A and Sirius B G140M Lyman α lines was lower than $\pm 5 \text{ km s}^{-1}$. The two corrected spectra in this range from Sirius A and Sirius B are plotted on the Fig. 6. Interstellar absorption lines are detected at the bottom of the photospheric Lyman α of both stars.

As one can see on the magnification of these two lines (see Fig. 7), however the profiles of the interstellar Lyman α lines are not the same toward Sirius A and Sirius B. The deuterium feature is detected on the blue wing toward both stars, but it is more contrasted on the Sirius B spectrum. The interstellar Lyman α line toward Sirius A seems to be more extended in the blue wing by at least 10 km s^{-1} . In the same way, the red wing of the Sirius B interstellar Lyman α is more extended by at least 50 km s^{-1} compared to the one toward Sirius A.

The differences between the two Lyman α interstellar absorption profiles are not caused by a simple instrumental wavelength shift. Indeed, the sizes of the extend differences are greater than the precision on the relative velocity ($\pm 5 \text{ km s}^{-1}$), which is confirmed by the relatively

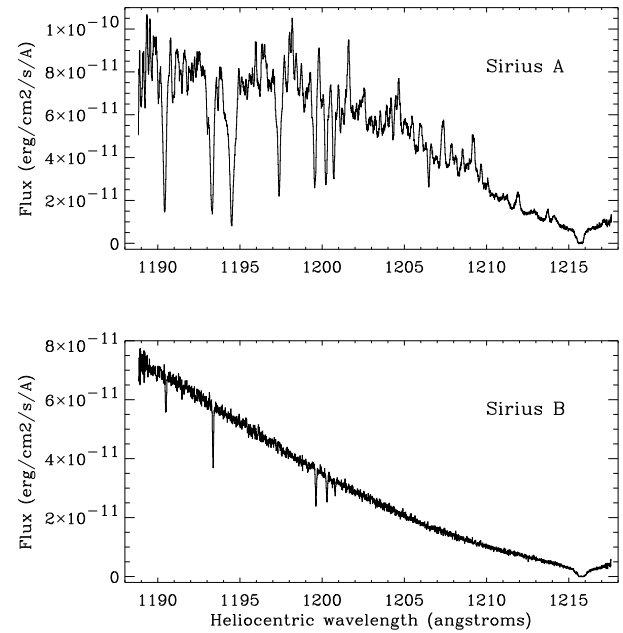


Fig. 6. G140M spectra of the Lyman α region of Sirius A (top) and Sirius B (bottom). Emission lines in the blue wing of the Sirius A Lyman α profile was studied by van Noort et al. (1998). Superimposed on the photospheric Lyman α absorption lines of the both stars are the lines Si II (1190 Å and 1193 Å) and N I (triplet at 1200 Å). Whereas the origin of these five lines is interstellar toward Sirius B, they are photospheric toward Sirius A, the interstellar components being not resolved. Only the interstellar Lyman α line is resolved both toward Sirius A and Sirius B on these spectra, at the bottom of the photospheric Lyman α lines, near 1216 Å on both plots.

good superposition of the two deuterium lines on the blue wings of Lyman α . Moreover, beyond the extent difference, the shape difference of the two profiles allows us to affirm that it is not a simple shift.

Comparing the high spectral resolution spectra of the C II 1334 Å and O I 1302 Å interstellar absorption lines, we did not detect such profile difference between Sirius A and Sirius B as in the case for the 1200 Å N I triplet lines. The N I triplet observations toward Sirius A, however, have a low S/N .

We thus observed an absorption excess in the blue wing of the Lyman α interstellar line toward Sirius A, and an absorption excess in the red wing of the Lyman α interstellar line toward Sirius B. These two excesses are only detected in the Lyman α line.

The two stars being separated by less than 4 arcsec on the sky at the time of our observations, which corresponds to ~ 10 AU at the Sirius distance of 2.6 pc, the processes which cause these excesses are likely due to the stars themselves, or to circumstellar material very close to the stars. Processes having origins in interstellar or interplanetary

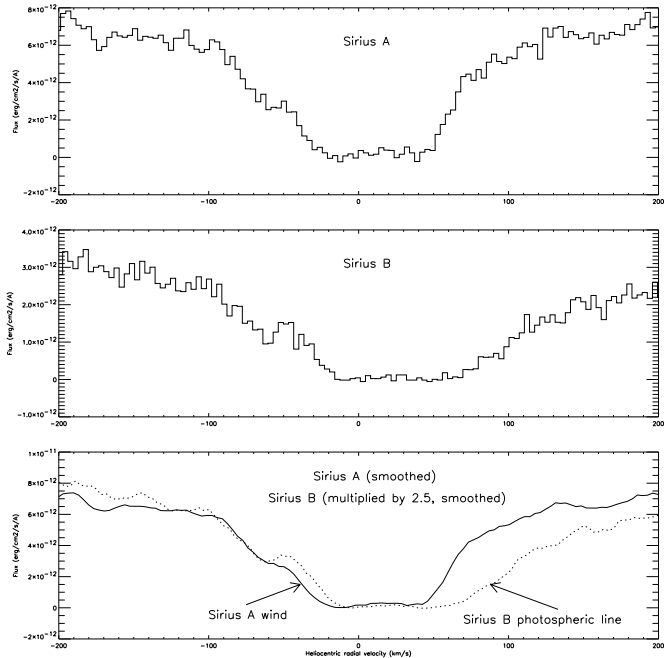


Fig. 7. Comparison of the Lyman α interstellar absorption lines toward Sirius A and Sirius B.

Top plot: Sirius A Lyman α line with G140M. Deuterium absorption is visible on the blue wing of the Lyman α line, near -60 km s^{-1} .

Middle plot: Sirius B Lyman α line with G140M. Compared to the Sirius A one, the deuterium absorption is more contrasted, and the red wing of the Lyman α line is more extended.

Bottom plot: Sirius A (solid line) and Sirius B (dotted line) smoothed spectra (overplot of the both above spectra). The flux of the Sirius B spectra is here multiplied by 2.5 to overlap the Sirius A one. Instrumental velocity shift between these two spectra are smaller than $\pm 5 \text{ km s}^{-1}$. That is confirmed by the good superposition of the two deuterium lines on this plot. The absorption excess in the blue wing of the Sirius A Lyman α line is interpreted as signature of stellar wind from Sirius A, and the absorption excess in the red wing of the Sirius B Lyman α line as signature of the white dwarf photospheric absorption Lyman α line.

media, or even in Earth environment, are very unlikely in order to explain differences on such small scales.

We interpret these signatures in the Lyman α profiles as stellar wind from Sirius A and of the core of the Sirius B Lyman α photospheric absorption line respectively, both superimposed on the classic interstellar feature. In § 4.1 and § 4.2 we discuss further these interpretations.

4.1. The Sirius B photospheric Lyman α line

Photospheric lines from Sirius B must be centered near 70 km s^{-1} (heliocentric). Indeed, the gravitational red-

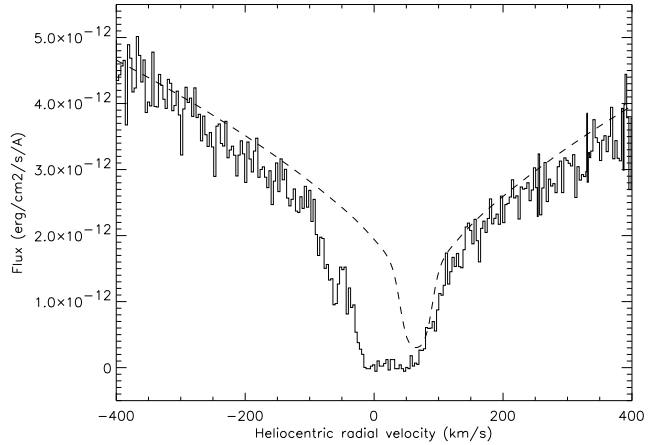


Fig. 8. Lyman α photospheric continuum for Sirius B. The model (dashed line) is shifted by 65 km s^{-1} to fit the data (solid line).

shift, measured by Greenstein et al. (1971) at $89 \pm 16 \text{ km s}^{-1}$ (note that the value obtained theoretically using the mass and radius is about 81 km s^{-1}), have to be corrected by the proper and orbital velocities of the white dwarf, which was about -20 km s^{-1} for the sum of both motions at the epoch of observation [orbital data of Sirius B by Couteau & Morel can be found in Benest & Duvent (1995)]. As seen in Fig. 7, the velocity position of the red absorption excess of the Sirius B Lyman α line is of this order of magnitude and may explain the excess by the Doppler core of the Lyman α photospheric absorption from Sirius B. This explanation requires fewer assumptions than any other, like infall on the white dwarf, for example.

We fit the Sirius B Lyman α photospheric profile by LTE and NLTE models calculated by the team of D. Koester using the very accurate parameters that Holberg et al. (1998) have derived for Sirius B: effective temperature $T_{\text{eff}} = 24790 \text{ K}$ and surface gravity $\log g = 8.57$. As seen in Fig. 7, the core of the Lyman α Sirius B photospheric line falls very near the zero flux level, perhaps even reaches it. We thus choose the model which presents the deepest core, *i.e.* the NLTE model. The best velocity shift found to fit the data is $v = 65 \text{ km s}^{-1}$, with an estimated uncertainty of $\pm 15 \text{ km s}^{-1}$. The plot of the fit is shown on Fig. 8.

The observed Sirius B Lyman α spectrum normalized by this model must thus show only the interstellar absorption due to both BC and LIC clouds identified in § 3.2. With the stellar continuum shape being uncertain, and the velocity shift (65 km s^{-1} , see Fig. 8) not determined better than $\pm 15 \text{ km s}^{-1}$, the red wing of this normalized interstellar line is very uncertain. However it is superimposed rather well on the red wing of the Sirius A Lyman α line, as expected if our interpretation is right.

The Sirius B Lyman α blue wing on the other hand is well known, since the stellar continuum is relatively flat on this part. This is the blue wing we will use below for the “pure interstellar” spectrum (§ 4.3).

4.2. Confirmation of the stellar wind from Sirius A

Bertin et al. (1995b) have reported earlier the feature in the blue wing of the interstellar Lyman α line toward Sirius A, and interpreted it as due to stellar wind. Our confirmation of this observation toward Sirius A and the fact that we do not observe this feature toward Sirius B is in agreement with this interpretation.

The comparison of the blue wings of the Lyman α lines of Sirius A and Sirius B could allow to estimate the shape of the absorption due to the wind, at least its blue part, its red part being lost in the saturated core of the two Lyman α lines. The wind absorption ranges at least from -10 to -60 km s^{-1} , in the range where Bertin et al. (1995b) detected it.

The wind absorption velocity distribution may be guessed assuming the velocity is in the rest frame of Sirius A at its surface and increases its blue shift outwards until it reaches a velocity limit. However, the abundance of neutral relative to ionized hydrogen probably changes with distance from the star.

Thus fits of the Sirius A wind absorption using a simple Voigt profile with a given velocity is too naive and could not give credible results. The study of the blue absorption feature is beyond the scope of the present work and will be the subject of a forthcoming paper.

4.3. The interstellar D/H ratio in the line of sight of Sirius

If both absorption excesses actually have a stellar origin, the interstellar part of the Lyman α line toward Sirius is at most the overlap between these two lines. Since each of the suspected processes that affect one wing of the Lyman α line cannot affect the other wing, we assumed that the interstellar contribution to the Lyman α line on this line of sight, generated by the interstellar clouds BC and LIC found in § 3.2, is the overlap between these two lines (see below).

The Sirius A Lyman α spectral region was normalized to unity by using a second degree polynomial stellar continuum [degree and parameters of that polynomial were found using the procedure described in Lemoine et al. (1995)]. Using that Sirius A Lyman α normalized spectrum and the Sirius B Lyman α spectrum normalized by the photospheric model (see § 4.1 and Fig. 8), we constructed a composit spectrum from the overlap of the two normalized spectra, *i.e.* with the blue wing of the Sirius B Lyman α line and the red wing of the Sirius A one. If our interpretations of the two excesses are correct, and if there are no other components in the interstellar Lyman α line

than the two indentified in the metal lines in § 3.2, this “pure interstellar” spectrum presents absorption caused only by H I and D I from the BC and LIC and is free of any other processes.

We fit the “pure interstellar” spectrum in order to determine the H I and D I column densities in BC and LIC, and thus the D/H ratio in the two interstellar clouds. In these fits, we fixed the values for the radial velocity shift, the temperatures and the turbulent velocities of both interstellar clouds found using the 19 metal lines fit as described in § 3.2 (see Table 3).

The first fit gave a $(\text{D}/\text{H})_{\text{LIC}}$ ratio in agreement with the Linsky et al. (1995) value of $(\text{D}/\text{H})_{\text{LIC}} = 1.60 \pm 0.09^{+0.05}_{-0.10} \times 10^{-5}$, obtained toward Capella and Procyon, but a surprising $(\text{D}/\text{H})_{\text{BC}}$ ratio about one order of magnitude lower, caused by a very low deuterium column density in the BC. We thus adopted in a first attempt the conservative method of adding an extra constraint by fixing the standard value $(\text{D}/\text{H})_{\text{LIC}} = 1.6 \times 10^{-5}$ in our Lyman α fits, and to let $(\text{D}/\text{H})_{\text{BC}}$ free in order to study this ratio. We found then $(\text{D}/\text{H})_{\text{BC}} < 0.5 \times 10^{-5}$.

The critical point which caused this very low D/H ratio is the D I column density in the BC, which should not easily exceed $1 \times 10^{12} \text{ cm}^{-2}$ in the frame of our assumptions and as indicated by the χ^2 . A D/H ratio of order 1.6×10^{-5} in BC thus requires a very low H I column density in BC, implying a ratio $N_{\text{LIC}}(\text{H I})/N_{\text{BC}}(\text{H I}) \geq 10$. This comes in contrast to a ratio $N_{\text{LIC}}(\text{N I})/N_{\text{BC}}(\text{N I}) \simeq 1.4$, N I column densities being accurate because obtained from several non-saturated lines (it is not the case for O I). As N I is regarded as a rather good tracer of H I (Ferlet 1981), a ratio $N_{\text{LIC}}(\text{H I})/N_{\text{BC}}(\text{H I})$ between 0.5 and 4 seems more realistic.

In order to obtain the most accurate results, we investigated and estimated the effects of possible systematic errors in our fits, possibly related to the set of assumptions made.

The first cause of systematic uncertainty is the shape of the Lyman α continuum. Indeed, as discussed in § 4.1, the normalization of the Sirius B Lyman α line, whose center lies in the blue wing of the “pure interstellar” Lyman α line, depends on both the choice of the stellar model and the velocity shift of the photospheric line, which is not known to better than $\pm 15 \text{ km s}^{-1}$. Whereas the “pure interstellar” spectrum was previously fitted without allowing the continuum level to vary during the fitting routine (the continuum was fixed at unity), we then added more freedom by having a 3rd order polynomial in order to fit the stellar continuum, this polynomial being fitted simultaneously with the Voigt functions (see Fig. 9). Because the new corrected continuum is close to unity and H I and D I column densities are similar to the ones found previously, this eliminates hidden systematics in the continuum as a serious compromise in our fit. In addition one should note that the inaccuracy of the fit related to the Sirius B

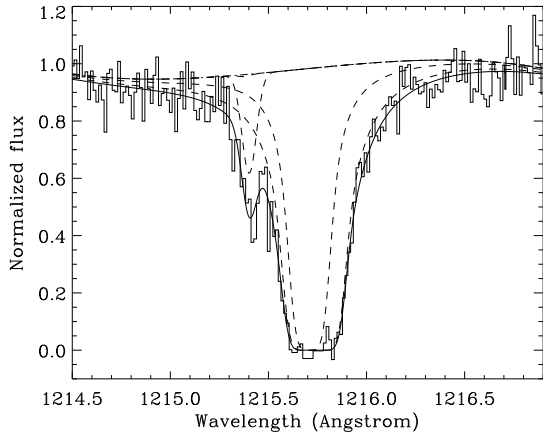


Fig. 9. Fit of the “pure interstellar” Lyman α line toward Sirius by a Voigt profil, the stellar continuum being fitted by a 3rd order polynomial. The continuum polynomial obtained is close to unity and interstellar column densities are close to those found if the stellar continuum is assumed to unity. Thus, systematic uncertainty in the stellar continuum does not seem to imply a serious uncertainty on our result. The spectrum fitted in Fig. 11 and Fig. 12 is normalized by this 3rd order polynomial.

photospheric Lyman α line does not affect significantly the blue wing of the “pure interstellar” line, as already mentioned in § 4.1. Although this correction was tiny, we normalized the “pure interstellar” spectra by this 3rd order polynomial to erase as well as possible the systematics related to the profile, which may mimic interstellar damping wings.

A second cause of systematic uncertainty is the instrumental velocity shift between the Sirius A and Sirius B G140M Lyman α lines, which can be $\pm 5 \text{ km s}^{-1}$, as seen above. The shape of the “pure interstellar” Lyman α line is compromised by this uncertainty. In order to quantify this effect we constructed two other “pure interstellar” spectra, one in which both wings of the Lyman α were 5 km s^{-1} nearer in comparison with the nominal spectra, and one in which they were 5 km s^{-1} more distant. The fits of these two spectra did not provide very different results, and again produced a low $(\text{D/H})_{\text{BC}}$ ratio.

We also estimated the influence of the zero flux level on the result. By studying χ^2 variations as a function of different zero flux levels, we found that the zero level of this saturated line is known to $\pm 3\%$ of the continuum flux level, in agreement with our previous estimation (see § 2.2). Fitting lines with zero levels 3% higher or 3% lower gave again very similar result, with low $(\text{D/H})_{\text{BC}}$ ratio.

The last systematic which we studied is the effect of the uncertainty on the structure of the sightline. Indeed, we fix in the fitting of the Lyman α line the values: $T_{\text{BC}} = 3000 \text{ K}$, $T_{\text{LIC}} = 8000 \text{ K}$, $\sigma_{\text{BC}} = 2.7 \text{ km s}^{-1}$, $\sigma_{\text{LIC}} = 0.5 \text{ km s}^{-1}$, and $\Delta v_{\text{LIC-BC}} = 5.9 \text{ km s}^{-1}$, found in § 3.2 by the study of

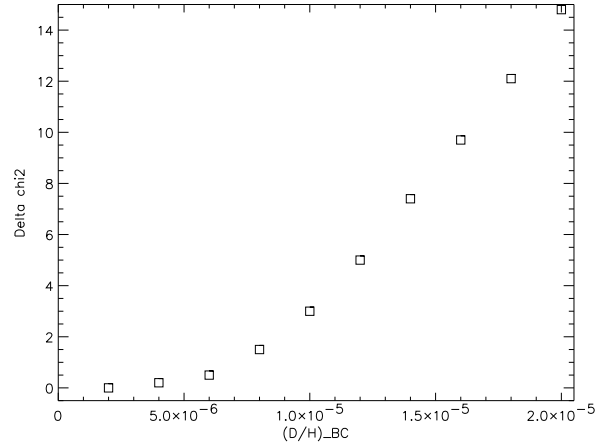


Fig. 10. $\Delta\chi^2$ as a function of $(\text{D/H})_{\text{BC}}$ [$(\text{D/H})_{\text{LIC}}$ being fixed at $= 1.6 \times 10^{-5}$]. The fits are made on the “pure interstellar” spectrum. The criterion $0 < \Delta\chi^2 < 10$ allow the range $0 < (\text{D/H})_{\text{BC}} < 1.6 \times 10^{-5}$.

metal lines. We used the error bars on T , σ and $\Delta v_{\text{LIC-BC}}$ reported in Table 3 to perform extra fits with different constraints, *i.e.* with components more or less broad, or more or less shifted from each other. Once again, we found similar results and low $(\text{D/H})_{\text{BC}}$ ratio.

Whereas all these tests allowed us to estimate systematic error bars, we evaluated statistical errors by the $\Delta\chi^2$ method, fixing the $(\text{D/H})_{\text{BC}}$ to a value, and looking for the best χ^2 for this given value, and iterating. The evolution of $\Delta\chi^2$ as a function of $(\text{D/H})_{\text{BC}}$ is reported on Fig. 10. Following the same criterion as Vidal-Madjar et al. (1998), we obtain $\Delta\chi^2=10$ for $(\text{D/H})_{\text{BC}} = 1.6 \times 10^{-5}$. This statistical error is rather large, due to the relatively low S/N and spectral resolution. Possible systematic effects discussed above are thus negligible in comparison with this statistical uncertainty. However, we were able to apply this $\Delta\chi^2$ method only to the “pure interstellar” spectrum, even though the blue wing of the Sirius A Lyman α contains some information, and in particular also prohibits too high $(\text{D/H})_{\text{BC}}$ values.

We note that comparing many lines of sight through the LIC, Linsky (1998) recently estimates a mean value of $(\text{D/H})_{\text{LIC}} = 1.50 \times 10^{-5} \pm 0.10$. If we assume that value, we obtain $\Delta\chi^2=10$ for $(\text{D/H})_{\text{BC}} = 1.7 \times 10^{-5}$.

We finally completed another study by fitting the “pure interstellar” Lyman α spectrum by relaxing the constraints on $(\text{D/H})_{\text{LIC}}$, and assuming that the D/H ratio is free but the same in the two components, in order to find which unique D/H ratio is compatible with our data. While keeping a $N_{\text{LIC}}(\text{H I})/N_{\text{BC}}(\text{H I})$ close to unity as above, we found that unique ratio to be $\text{D/H} = 1.2 \times 10^{-5}$. Although we cannot exclude this result, this fit is significantly worse with a same D/H ratio in both clouds, rather

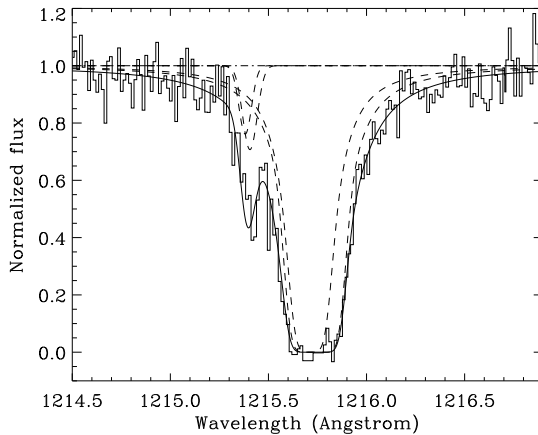


Fig. 11. Fit of the “pure interstellar” Lyman α line assuming $(D/H)_{\text{LIC}} = (D/H)_{\text{BC}} = 1.6 \times 10^{-5}$. The quality of the fit in the blue wing of the line is degraded in that case in comparison with the case assuming a lower $(D/H)_{\text{BC}}$ ratio (see Fig. 12).

than with two different ones as above. Fits with higher common D/H ratios (1.4 or 1.6×10^{-5}) degrade even more the quality of the fit (see Fig. 11) and could be rejected in term of χ^2 . These data seems thus to reject the possibility of a unique $(D/H)_{\text{ISM}}$ ratio in both components although marginally.

In brief, the results which we obtained in terms of H I and D I column densities, and D/H ratios, for the BC and the LIC are summarized in Table 4. The range which we finally obtain in the Blue Component for the deuterium abundance is $0 < (D/H)_{\text{BC}} < 1.6 \times 10^{-5}$. The upper limit $(D/H)_{\text{BC}} < 1.6 \times 10^{-5}$ corresponds to a $\Delta\chi^2 = 10$ in comparison with the lowest χ^2 obtained for $(D/H)_{\text{BC}} < 0.5 \times 10^{-5}$. Thus we found that the deuterium abundance could be equal to 1.6×10^{-5} in LIC and BC, but with a low probability according to our data. Moreover our $\Delta\chi^2$ was obtained from the “pure interstellar” spectrum. Although we were unable to fit the deuterium Sirius A line because of the stellar wind feature, that line shows also that the deuterium column density could not be too high. That suggests a lower upper limit for $(D/H)_{\text{BC}}$.

Fig. 12 shows one of the best fits of the “pure interstellar” spectrum which we obtained, with the values $(D/H)_{\text{LIC}} = 1.6 \times 10^{-5}$ and $(D/H)_{\text{BC}} = 0.5 \times 10^{-5}$.

4.4. No-confirmation of the detection of a diffuse cloud boundary

Bertin et al. (1995a) reported the detection of excess absorption in the red wing of the Sirius A Lyman α line and interpreted it as being due to a warmer very diffuse neutral

Table 4. H I and D I column densities in BC and LIC clouds obtained by fitting of the “pure interstellar” Lyman α line (see fit in Fig. 12).

Component	BC	LIC
$N(\text{H I}) [\text{cm}^{-2}]$	$2.5_{-1.0}^{+1.0} \times 10^{17}$	$4.0_{-1.0}^{+1.5} \times 10^{17}$
$N(\text{D I}) [\text{cm}^{-2}]$	$1.0_{-1.0}^{+2.0} \times 10^{12}$	$6.5_{-1.5}^{+1.5} \times 10^{12}$
D/H	$0.5_{-0.5}^{+1.1} \times 10^{-5}$	$1.6_{-0.4}^{+0.4} \times 10^{-5}$

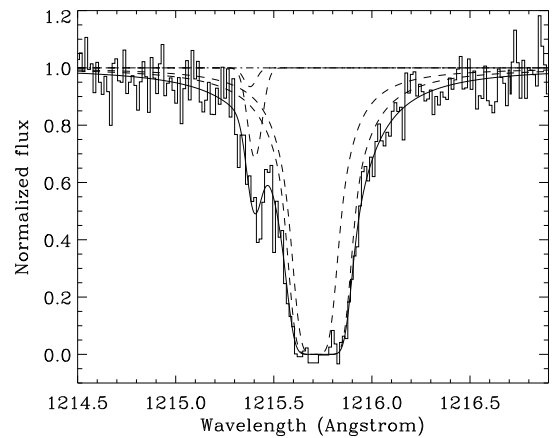


Fig. 12. Final fit of the “pure interstellar” Lyman α line toward Sirius, in which radial velocity shift $\Delta v_{\text{LIC-BC}}$, temperatures and turbulent velocities of BC and LIC are fixed from Table 3. $(D/H)_{\text{LIC}}$ is fixed at 1.6×10^{-5} , and $(D/H)_{\text{BC}}$ at 0.5×10^{-5} .

region, which may originate from an evaporative interface between the hot “Local Bubble” and the warm interstellar gas. Izmodenov et al. (1999) proposed to explain that red excess in a different way, by the absorption of the neutralized, compressed solar wind from the heliosheath in the downwind direction.

We do not detect in our data the signature of that third absorber previously seen by Bertin et al (1995a) in the Sirius A Lyman α line, despite very similar Lyman α profiles. This disagreement is neither due to a difference between the two spectra, caused for example by possible errors in the different data reduction procedures used for the different data sets gathered toward Sirius A using the G160M grating (Bertin et al. 1995a) and the G140M grating (our case), nor by real changes in the stellar line profile since both our Lyman α Sirius A spectra are very similar. It is due to a different analysis of two almost identical spectra. In effect, the cause of this disagreement comes from the different D I column densities we derive for the two

components thanks to the Sirius B Lyman α observation (clean over the D I line), compared to the ones evaluated by Bertin et al. (1995a) from Sirius A Lyman α alone. Indeed Bertin et al. (1995a) evaluated D I column densities from Sirius A first, and derived H I column densities using the Linsky et al. (1993) (D/H)_{ISM} ratio as a unique common value. In addition to the fact that we do not find the same (D/H)_{ISM} ratio for the two components, we argue that the D I column densities obtained from Sirius A Lyman α line are less reliable than those obtained from Sirius B Lyman α line because of the blue excess observed toward Sirius A. This excess, located near the wavelength of D I, casts some doubts on the determination of the D I column density by Bertin et al. (1995a).

In effect we found a total D I column density 1.4 times larger than the one found by Bertin et al. (1995a) and, according to our composite profile, a total H I column density 1.9 times larger. This explains the differences between the two studies. Bertin et al. (1995a) also noticed that the H I total column density they found was smaller than other evaluations in short lines of sight and in particular to the one obtained by Bruhweiler & Kondo (1982) toward Sirius B from the N I column density using IUE: $N(\text{H I}) = 8.5 \times 10^{17} \text{ cm}^{-2}$. Here we find a slightly lower total column density $N(\text{H I}) \sim 6.5 \times 10^{17} \text{ cm}^{-2}$. Our value however agrees well with the recent result by Holberg et al. (1998) who found toward Sirius B, from Si II, O I and C II column densities: $N(\text{H I}) = 5.2^{+1.4}_{-1.1} \times 10^{17} \text{ cm}^{-2}$.

In addition, we note that Izmodenov et al. (1999) propose to explain the absorption excess in the blue wing of the Lyman α line toward Sirius A by hydrogen atoms formed in an *astrosphere* around Sirius, similar to the *heliosphere* around the Sun. However, our data obtained toward Sirius B show that we do not observe such a blue excess toward the Sirius A companion. The two stars being separated by ~ 10 AU at the time of our observations and the *siriosphere* having a size of about 200 AU, the *siriosphere* absorption should have been observed toward Sirius A and Sirius B with similar amounts of absorption. The fact that we observe it only toward Sirius A favours the stellar wind interpretation rather than the *siriosphere* one. The Sirius A wind proposed by Bertin et al. (1995b) is thus the more probable explanation since it was also detected in the Mg II doublet.

5. Analysis of the metal lines

In this section we discuss briefly the abundances measured in the metal lines.

5.1. C, N, O and Si abundances and depletions

Any discussion in the abundances and depletion level of C, N, O and Si is compromised by the uncertainties in the column density of H I (especially of BC) and the metal lines (especially C II).

Table 5. Depletion factors relative to solar values (*i.e.* solar abundance divided by measured interstellar abundance). Solar abundances are from Anders & Grevesse (1989).

	BC	LIC		BC	LIC
N I/H I	2.6	4.2	—	—	—
O I/H I	2.7	0.9	O I/N I	1.1	0.2
Si II/H I	2.3	5.0	Si II/N I	1.1	1.2
C II/H I	1.2	0.4	C II/N I	0.5	0.1
Fe II/H I	19.0	13.8	Fe II/N I	3.7	3.3
Mg II/H I	6.7	9.0	Mg II/N I	2.6	2.2

Nonetheless, comparing the column densities of the N I, O I, Si II and C II lines of the BC and the LIC relative to their respective H I values, we determined the depletion factors as listed in Table 5.

For BC, N I, O I and Si II show a depletion factor relative to the solar one (Anders & Grevesse 1989) of ~ 2.5 whereas C II is depleted by a smaller factor of ~ 1.2 . For LIC, N I and Si II show a depletion factor of ~ 4.5 , C II is over abundant by a factor 2.5. In LIC, as opposed to BC, O I does not show a similar depletion to N I and Si II.

Instead of comparing column densities to H I we used N I, assuming N I traces H I well. We find depletions as shown in Table 5. Again C II and O I interstellar abundances appear too high in the LIC.

Linsky et al. (1995) measured in the LIC toward Capella $10^6 \times N(\text{O I})/N(\text{H I}) \simeq 480$ from GHRS observations. Meyer et al. (1998) derived from GHRS observations the accurate average ISM gas neutral abundance $10^6 \times N(\text{O I})/N(\text{H I}) = 319 \pm 14$. Our values obtained in BC and LIC are respectively 200^{+100}_{-130} and 850^{+360}_{-270} , so the O I column density which we obtained in the LIC appears be higher than other evaluations.

About N I, Meyer et al. (1997) derived the average ISM abundance $10^6 \times N(\text{N I})/N(\text{H I}) = 75 \pm 4$, which is more accurate than the one obtained by Ferlet (1981): $10^6 \times N(\text{N I})/N(\text{H I}) = 62^{+45}_{-34}$. We obtained inside BC and LIC 37 ± 15 and 32 ± 7 respectively, which appear to be low values, although compatible with the Ferlet (1981) value. We note that already Vidal-Madjar et al. (1998) found a low N I abundance on average toward G191-B2B: $10^6 \times N(\text{N I})/N(\text{H I}) = 33 \pm 2$. This seems to confirm a rather low N I content in the local ISM relative to the average ISM value.

On the other hand, column densities of C II and O I in the LIC appear too high. These two lines being saturated and not clearly showing the two components as other metal lines, it could mean that the column densities derived for C II and O I are slightly overestimated.

5.2. Ionization of the Local Interstellar Cloud

We obtained four spectra on the spectral region of the 1334 Å C II line, toward Sirius A or Sirius B with high

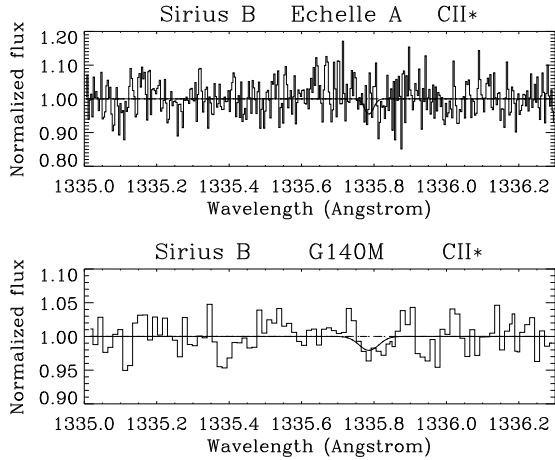


Fig. 13. High (top) and medium (bottom) resolution normalized spectra of the C II* line at 1335.7 Å toward Sirius B. The thick solid line corresponds to the limiting 1.5 mÅ detectable equivalent width at 3σ . The interstellar line is not significantly detected.

and medium spectral resolution. We did not significantly detect the interstellar excited-state C II* line at 1335.7 Å. Assuming the above results for the width of the LIC lines, the criterion on the limiting detectable equivalent width at 3σ [$W_{lim} \equiv \frac{3\Delta\lambda}{S/N}$, see Hébrard et al. (1997)] gives the lower value $W_{lim} \simeq 1.5$ mÅ on Sirius B spectra (see Fig. 13) and the upper limit of $N_{LIC}(\text{C II}^*) \leq 8 \times 10^{11} \text{ cm}^{-2}$ [assuming $f_{\text{C II}^*} = 0.1149$ (Morton 1991)]. We thus obtained:

$$\left[\frac{N(\text{C II}^*)}{N(\text{C II})} \right]_{\text{LIC}} \leq 3 \times 10^{-3}.$$

Wood & Linsky (1997) used this ratio to derive the electron density from the equation of the equilibrium between collisional excitation to excited-state C II* and radiative de-excitation to ground-state C II:

$$N(\text{C II}^*) \times A_{21} = N(\text{C II}) \times n_e C_{12}(T).$$

These authors derive the value $n_e = 0.11_{-0.06}^{+0.12} \text{ cm}^{-3}$ for the LIC toward Capella. Using the same method toward the white dwarf REJ 1032-532, Holberg et al. (1999) derive the same value for the LIC: $n_e = 0.11_{-0.06}^{+0.07} \text{ cm}^{-3}$. Our non-detection of C II* in the LIC toward Sirius gives the limit $n_e \leq 0.05 \text{ cm}^{-3}$, following Wood & Linsky (1997) and references therein in order to find the value for the radiative de-excitation rate coefficient A_{21} and determine the value of the collision rate coefficient $C_{12}(T)$ for $T=8000$ K. Wood & Linsky (1997) used the value $T=7000$ K, which is the temperature usually found for the LIC. Using $T=7000$ K in our calculation leads to a very slightly and non-significantly lower value for n_e compared to the one obtained using $T=8000$ K.

This low value of n_e indicates a rather low ionization, which could be argued for also by the non-detection of the

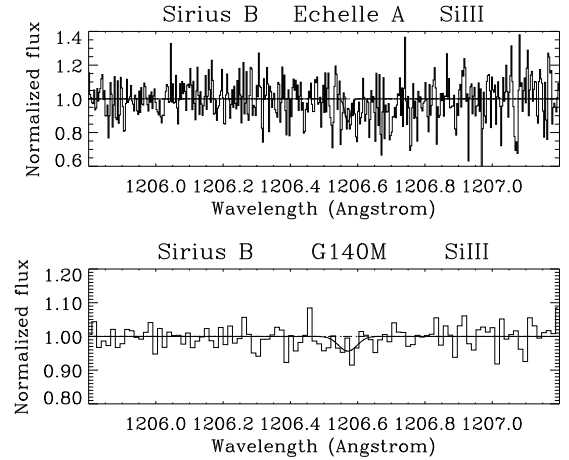


Fig. 14. High (top) and medium (bottom) resolution normalized spectra of the Si III line at 1206.5 Å toward Sirius B. The thick solid line corresponds to the limiting 3 mÅ detectable equivalent width at 3σ . The interstellar line is not significantly detected.

Si III interstellar line at 1206.5 Å. The Sirius A Si III photospheric line appears near 0 km s^{-1} but no interstellar Si III line is significantly detected on any of our four spectra in that spectral region, toward Sirius A or Sirius B with high and medium spectral resolution. The lower limiting detectable equivalent width at 3σ found, obtained on Sirius B spectra (see Fig. 14), is $W_{lim} \simeq 3$ mÅ, from which we derive the upper limit $N_{LIC}(\text{Si III}) \leq 1.5 \times 10^{11} \text{ cm}^{-2}$ [assuming $f_{\text{Si III}} = 1.669$ (Morton 1991)]. We thus obtained:

$$\left[\frac{N(\text{Si III})}{N(\text{Si II})} \right]_{\text{LIC}} \leq 6 \times 10^{-2}.$$

This non-detection of the line Si III at 1206.5 Å is surprising because this line was detected in the LIC by Gry et al. (1995) toward ϵ CMa which is located only 12° away from Sirius. They derived the column density $N_{LIC}(\text{Si III}) = 2.0 \pm 0.2 \times 10^{12} \text{ cm}^{-2}$ which is a value more than 10 times larger than our upper limit! If the line detected by Gry et al. (1995) is actually caused by the LIC and not by another more distant cloud whose radial velocity is by coincidence confused with the LIC one, this may mean that the ionization in the LIC varies over very short distances. This non-detection may confirm the non-detection of Si III in the LIC already reported toward G191-B2B by Vidal-Madjar et al. (1998). Moreover, Holberg et al. (1999) claimed that it is quite doubtful that the Si III ISM absorption line that they detected toward REJ 1032-532 is produced in the LIC. Thus it seems to favour the idea that another cloud in the long line of sight toward ϵ CMa is by coincidence at a radial velocity similar to the LIC one. Note that Gry et al. (1995) do not detect Si III in their “component 2”, in agreement with our non-detection of that ion in “BC” toward Sirius, which is identified as the same component.

In addition, Dupin & Gry (1998) detected a saturated Si III line at 1206.5 Å in their component “D” toward β CMa, which is located at less than 6° from Sirius. They derived the column density $N(\text{Si III}) = (1.5 - 10) \times 10^{14} \text{ cm}^{-2}$. Since the velocity of that component does not correspond to the LIC, this huge Si III column density could be interpreted as a sign that the component “D”, detected by Dupin & Gry (1998) toward β CMa, is probably located beyond Sirius and may explain some Si III absorption in the ϵ CMa line of sight, for instance at the LIC velocity.

6. Discussion

Our D/H evaluation is made assuming the three following main hypotheses:

- The structure of the interstellar medium is the same toward Sirius A and Sirius B. Thus we detect the same interstellar clouds with the same physical properties toward these two targets.
- The H I and D I interstellar structure at Lyman α is the one determined through the O I, N I, Si II, C II, Fe II and Mg II lines. Then the physical properties (temperature, turbulence, velocity) at Lyman α are the same as in the metal lines, and there is no extra H I or D I interstellar component in addition to the BC and the LIC.
- The processes which are responsible for the extra absorption in the blue wing of the Lyman α line toward Sirius A and in the red wing of the Lyman α line toward Sirius B are from stellar origin and do not perturb the BC and LIC absorptions. In addition, each process on each Lyman α wing does not reach the other wing. Thus, the composite Lyman α line formed by the red wing of the Sirius A and the blue wing of the Sirius B is a “pure interstellar” Lyman α line, and presents absorptions caused only by the BC and LIC.

The first assumption is justified by the small distance between the two stars (~ 10 AU). The second assumption is less strongly justified and one can imagine a low column density H I component without detectable metal line, but with a still significant absorption at Lyman α . The most we can argue is that it is possible to fit the “pure interstellar” Lyman α line only with the BC and the LIC as found with the metal lines and that no extra component is required by the data. We did not find any width or velocity structure unexplained by our simple interstellar model (*i.e.* only two components), as Linsky & Wood (1996) did *e.g.* on the sightline of α Cen. This led them to the detection of an extra H I component they called the “hydrogen wall”. We are however unable to formally exclude the presence of additional low H I column density clouds. The third assumption is justified again by the proximity between the two targets whereas their Lyman α absorptions are very different. This favours processes linked to

the stars as causes of the extra Lyman α absorptions. Finally these suspected processes, the wind from Sirius A and the Sirius B photospheric line shape, are unable to disturb the other wing of the Lyman α line.

The reliability of our result is linked to the robustness of these hypotheses and to the possible inaccuracy in the metal column densities, as described in the § 5.1. We can note however that the C II and O I column densities, suspected to be too high, do not seriously constrain the Lyman α fit. Indeed, the radial velocity shift of 5.9 km s^{-1} between BC and LIC applied to the Lyman α line is essentially constrained by the Fe II, Mg II and N I lines which only show clearly the BC and LIC components. Moreover, we used N I and not O I as tracer of H I, in order to argue that the H I column density ratio between LIC and BC should be probably ranging between 0.5 and 4. We thus concluded that possible inaccuracies in the C II and O I column densities do not affect our $(\text{D/H})_{ISM}$ evaluation.

Although the value of $(\text{D/H})_{BC}$ could be between 0 and 1.6×10^{-5} , the best result is obtained with a low value. We found thus a $(\text{D/H})_{ISM}$ abundance which seems to be low in one of the two components (BC) toward Sirius without being able to find an artifact able to explain that result. O and N are not overabundant in this component. It is thus difficult to see BC as a cloud polluted by D free material ejected by the planetary nebula preceding the formation of the white dwarf Sirius B since furthermore its radial velocity should be blue-shifted, whereas the BC one is redshifted. This fact does not agree with the simple idea of BC being an expanding shell of material ejected by the planetary nebula related to the white dwarf Sirius B.

After G191-B2B (Vidal-Madjar et al. 1998) and δ Ori (Jenkins et al. 1999) on the line of sight of which low $(\text{D/H})_{ISM}$ were measured, Sirius seems to be a good candidate for finding another low interstellar deuterium abundance.

The cause of these variations has to be understood in order to know what is the actual value of the $(\text{D/H})_{ISM}$, if any. It is difficult to see interstellar deuterium as the simple tracer of the galactic chemical evolution. The study of its possible variation as a function of the radial distance to the galactic center may help us in that matter.

Moreover, if $(\text{D/H})_{ISM}$ ratio actually presents dispersion, one can argue that the other deuterium abundance evaluations, *i.e.* proto-solar and primordial abundances, can also present dispersion. Indeed, variations of interstellar abundance of deuterium was detected thanks to the large number of sightlines available (several tens), whereas proto-solar and primordial abundances are determined only from few targets. Taking into consideration this problem, observing deuterium in the interstellar medium toward a large number of sightlines is a good way to proceed.

7. Conclusions

We have presented new spectroscopic observations of Sirius A and Sirius B performed using HST-GHRS. 14 interstellar lines were detected at high and/or medium spectral resolution. The sightline, which is assumed to present the same structure toward the two stars, is composed by two clouds: the Blue Component (BC) and the Local Interstellar Cloud (LIC), in agreement with the previous HST-GHRS observations of Sirius A reported by Lallement et al. (1994).

The three main results of our observations are the following:

- The Lyman α lines do not present the same profile toward Sirius A and Sirius B, an extra absorption being observed in the blue wing of the Sirius A Lyman α line, and an extra absorption being observed in the red wing of the Sirius B Lyman α line. We interpreted these excesses respectively as the signatures of the wind from Sirius A and of the core of the Sirius B photospheric Lyman α line.
- A composite Lyman α profile was constructed from these two lines and fitted in order to measure the $(D/H)_{ISM}$ ratio on the two components. Our data are compatible with D/H ratio found in the LIC by Linsky et al. (1993 & 1995), *i.e.* $(D/H)_{LIC} = 1.60 \pm 0.09^{+0.05}_{-0.10} \times 10^{-5}$. Our result is $(D/H)_{LIC} = 1.6 \pm 0.4 \times 10^{-5}$. In the other component, BC, we did not detect a significant D I line. The ratio we derived is $0 < (D/H)_{BC} < 1.6 \times 10^{-5}$.
- We did not detect the interstellar absorption of Si III at 1206.5 Å and C II* at 1335.7 Å. This implies a low electron density n_e , for which we found the upper limit $n_e \leq 0.05 \text{ cm}^{-3}$ in the LIC, assuming equilibrium between collisional excitation to excited-state C II* and radiative de-excitation to ground-state C II. Since measured values of the electron density are higher in the LIC toward other sightlines, the new value of n_e toward Sirius could point to inhomogeneities in the Local Interstellar Cloud.

The data are thus consistent with $(D/H)_{BC}$ in the range 0 to 1.6×10^{-5} . The BC cloud is a candidate region for low $(D/H)_{ISM}$, but no definite conclusion about D/H can be made at this time. We intend to continue the study of the Sirius system until we can come to a definitive conclusion as to whether or not a low $(D/H)_{ISM}$ is present in the BC. In particular, it is critically important that this experiment be done again with deep HST-STIS observations to study the Lyman α line and FUSE observations to study the higher Lyman lines. FUSE, the Far Ultraviolet Spectroscopic Explorer which was launched on June 24, 1999, will perform observations between 905 and 1187 Å, at a spectral resolution of $R = \lambda/\Delta\lambda \simeq 30,000$. The primary goal of that mission is to observe deuterium toward more than one hundred targets, from the Solar Sys-

tem and the local interstellar medium up to extragalactic low-redshift objects. These dedicated studies should greatly clarify the problem of the chemical evolution of deuterium.

Acknowledgements. We thank L. Ben Jaffel and J.-P. Dumont for many stimulating discussions. We also thank S. Dreizler for the calculation of the NLTE profiles for Sirius B, and P. Couteau for informations about orbit of Sirius B around Sirius A. We would like to thank the STScI staff for rescheduling observations after an original failure. Especially, we are grateful to A. Berman who noticed that the plan for the repeated observations would probably also fail, D. Soderblom who proposed another approach that was successful, and A. Schultz who implemented it. Finally we would thank the referee J. Linsky for very useful and constructive comments. D.K. acknowledges support by grants from the DLR.

References

Allen, M.M., Jenkins, E.B., & Snow, T.P.: 1992, *ApJS* 83, 261
 Anders, E., Grevesse, N.: 1989, *Geochim. Cosmochim. Acta* 53, 197
 Benest, D., & Duvent, J.L.: 1995, *A&A* 299, 621
 Bertin, P., Vidal-Madjar, A., Lallement, R., Ferlet, R., & Lemoine, M.: 1995a, *A&A* 302, 889
 Bertin, P., Lamers, H.J.G.L.M., Vidal-Madjar, A., Ferlet, R., & Lallement, R.: 1995b, *A&A* 302, 899
 Bruhweiler, F.C., & Kondo, Y.: 1982, *ApJ* 259, 232
 Burles, S., & Tyler, D.: 1998a, *ApJ* 499, 699
 Burles, S., & Tyler, D.: 1998b, *ApJ* 507, 732
 Burles, S., & Tyler, D.: 1998c, *Proceedings of the Second Oak Ridge Symposium on Atomic & Nuclear Astrophysics*, ed. A. Mezzacappa (Institute of Physics, Bristol), to appear, [astro-ph/9803071](http://arXiv.org/abs/astro-ph/9803071)
 Chengalur, J.N., Braun, R., & Burton, W.B.: 1997, *A&A* 318, L35
 Duncan, D.: 1992, *Hubble Space Telescope Goddard High Resolution Spectrograph Instrument Handbook*, version 3.0, STScI
 Dupin, O., & Gry, C.: 1998, *A&A* 335, 661
 Epstein, R.I., Lattimer, J.M., & Schramm, D.N.: 1976, *Nature* 263, 198
 Ferlet, R.: 1981, *A&A* 98, L1
 Galli, D., Palla, F., Ferrini, F., & Penco, U.: 1995, *ApJ*, 443, 536
 Greenstein, J.L., Oke, J.B., & Shipman, H.L.: 1971, *ApJ* 169, 563
 Gry, C., Lemonon, L., Vidal-Madjar, A., Lemoine, M., & Ferlet, R.: 1995, *A&A* 302, 497
 Hébrard, G., Lemoine, M., Ferlet, R., & Vidal-Madjar, A.: 1997, *A&A* 324, 1145
 Holberg, J.B., Bruhweiler, F.C., Barstow, M.A., Dobbie, P.D.: 1999, *ApJ* 517, 841
 Holberg, J.B., Barstow, M.A., Bruhweiler, F.C., Cruise, A.M., & Penny, A.J.: 1998, *ApJ* 497, 935
 Izmodenov, V.V., Lallement, R., & Malama, Y.G.: 1999, *A&A* 342, L13
 Jenkins, E.B., Tripp, T.M., Woźniak, P.R., Sofia, U.J., & Sonneborn, G.: 1999, *ApJ* 520, 182, [astro-ph/9901403](http://arXiv.org/abs/astro-ph/9901403)

Jura, M.A.: 1982, *Four Years of IUE Research*, NASA CP 2238, 54

Lallement, R., & Bertin, P.: 1992, A&A 266, 479

Lallement, R., Bertin, P., Ferlet, R., Vidal-Madjar, A., & Bertaux, J.L.: 1994, A&A 286, 898

Laurent, C., Vidal-Madjar, A., & York, D.G.: 1979, ApJ 229, 923

Lemoine, M., Audouze, J., Ben Jaffel, L., Feldman, P., Ferlet, R., Hébrard, G., Jenkins, E.B., Mallouris, C., Moos, W., Sembach, K., Sonneborn, G., Vidal-Madjar, A., & York, D.G.: 1999, *New Astronomy* 4, 231, astro-ph/9903043

Lemoine, M., Vidal-Madjar, A., Bertin, P., Ferlet, R., Gry, C., & Lallement, R.: 1996, A&A 308, 601

Lemoine, M., Ferlet, R., & Vidal-Madjar, A.: 1995, A&A 298, 879

Linsky, J.L.: 1998, *Space Science Reviews* 84, 285

Linsky, J.L., & Wood, B.E.: 1996, ApJ 463, 254

Linsky, J.L., Diplas, A., Wood, B.E., Brown, A., Ayres, T.R., & Savage, B.D.: 1995, ApJ 451, 335

Linsky, J.L., Brown, A., Gayley, K., Diplas, A., Savage, B.D., Ayres, T.R., Landsman, W., Shore, S.W., & Heap, S.R.: 1993, ApJ 402, 694

Meyer, D.M., Jura, M., & Cardelli, J.A.: 1998, ApJ 493, 222

Meyer, D.M., Cardelli, J.A., & Sofia, U.J.: 1997, ApJ 490, L103

Morton, D.C.: 1991, ApJS 77, 119

Mullan, D.J., & Linsky, J.L.: 1999, ApJ 511, 502

Murthy, J., Henry, R.C., Moos, H.W., Landsmann, W.B., Vidal-Madjar, A., Linsky, J.L., & Gry, C.: 1990, ApJ 356, 223

Murthy, J., Henry, R.C., Moos, H.W., Landsmann, W.B., Linsky, J.L., Vidal-Madjar, A., & Gry, C.: 1987, ApJ 315, 675

Prantzos, N.: 1996, A&A 310, 106

Prantzos N.: 1995, in *Nuclei in the Cosmos III*, Eds M. Busso et al., AIP Conf. Proc., 327, 531

Reeves, H., Audouze, J., Fowler, W.A., & Schramm, D.N.: 1973, ApJ 179, 909

Rogerson, J., & York, D.: 1973, ApJ 186, L95

Scully, S.T., Cassé, M., Olive, K.A., & Vangioni-Flam, E.: 1997, ApJ 476, 521

Tosi, M., Steigman, G., Matteucci, F., & Chiappini, C.: 1998, ApJ 498, 226

Vangioni-Flam, E., Cassé, M.: 1995, ApJ 441, 471

van Noort, M., Lanz, T., Lamers, H.J.G.L.M., Kurucz, R.L., Ferlet, R., Hébrard, G., & Vidal-Madjar, A.: 1998, A&A 334, 633

Vidal-Madjar, A., Lemoine, M., Ferlet, R., Hébrard, G., Koester, D., Audouze, J., Cassé, M., Vangioni-Flam, E., & Webb, J.: 1998, A&A 338, 694

Vidal-Madjar, A., Ferlet, R., Gry, C., & Lallement, R.: 1986, A&A 155, 407

Vidal-Madjar, A., Laurent, C., Bruston, P., & Audouze, J.: 1978, ApJ 223, 589

Webb, J.K., Carswell, R.F., Lanzetta, K.M., Ferlet, R., Lemoine, M., Vidal-Madjar, A., & Bowen, D.V.: 1997, Nature 388, 250

Welty, D.E., Hobbs, L.M., & York, D.G.: 1991, ApJS 75, 425

Wood, B.E., & Linsky, J.L.: 1997, ApJ 474, L39

York, D.G.: 1983, ApJ 264, 17

York, D.G., Spitzer, L., Bohlin, R.C., Hill, J., Jenkins, E.B., Savage, B.D., & Snow, T.P.: 1983, ApJ 266, L55